Multi-orbital Non-Crossing Approximation from maximally localized Wannier functions: the Kondo signature of copper phthalocyanine on Ag (100)

Richard Korytár[1]

E-mail: `rkorytar@cin2.es`

Nicolás Lorente[1]

[1]Centro de investigación en nanociencia y nanotecnología (CSIC - ICN), Campus de la UAB, E-08193 Bellaterra, Spain

Abstract. We have developed a multi-orbital approach to compute the electronic structure of a quantum impurity using the non-crossing approximation. The calculation starts with a mean-field evaluation of the system's electronic structure using a standard quantum chemistry code. Here we use density functional theory (DFT). We transformed the one-electron structure into an impurity Hamiltonian by using maximally localized Wannier functions (MLWF). Hence, we have developed a method to study the Kondo effect in systems based on an initial one-electron calculation. We have applied our methodology to a copper phthalocyanine molecule chemisorbed on Ag (100), and we have described its spectral function for three different cases where the molecule presents a single spin or two spins with ferro- and anti-ferromagnetic exchange couplings. We find that the use of broken-symmetry mean-field theories such as Kohn-Sham DFT cannot deal with the complexity of the spin of open-shell molecules on metal surfaces and extra modeling is needed.

PACS numbers: 72.15.Qm, 72.10.Fk, 73.20.Hb, 75.20.Hr

1. Introduction

Since the study of the Kondo features of Ce ad-atoms on Ag (111)[1] and Co ad-atoms on Au (111) [2], the scanning tunnelling microscope (STM) has become a privileged tool in the study of surface Kondo physics. The STM is a non-intrusive probe that can address adsorbed objects at very low bias with very small currents. Hence, the STM basically explores the equilibrium properties of the adsorbed systems. Besides ad-atoms, Kondo physics has been revealed in objects of increasing complexity, from single adsorbates [1, 2, 3] to large organic molecules [4, 5, 6, 7, 8], ordered nanostructures [9] and ad-atom-ligand structures [10, 11].

Several recent reports show that organic molecules display a Kondo state due to a spin in their extended π-orbitals even when they are adsorbed on a metal surface [7, 8, 12, 13]. This is somewhat of a surprise for two reasons: (i) some of these molecules are magnetic in the gas phase because they have a magnetic atom, (ii) an extended π-orbital is expected to have a large overlap with the metal surface likely driving the π-system into a mixed valence regime instead of a Kondo one. Hence, the appearance of Kondo physics in these systems depends on a series of parameters where common wisdom is likely to fail. It is then of great interest to perform calculations to rationalize the particular features of adsorbed large molecules that depend as little as possible on adjustable parameters.

We have implemented an impurity solver for the Anderson Hamiltonian [14] that reads the one-electron structure from a density functional theory (DFT) calculation for a given spin configuration of the impurity (in the present case the molecular orbitals involved in the spin configuration), uses the DFT hybridization to compute the dynamical electron exchange with the substrate, and assumes a single electron fluctuation which corresponds to the $U \to \infty$ limit of the Anderson Hamiltonian. The impurity solver uses the non-crossing approximation NCA [15, 16, 17, 18] in the multi-orbital formalism by Kuramoto [16]. The multi-orbital aspects of the Kondo problem must be correctly taken into account in realistic accounts of the Kondo problem as shown by Kroha and collaborators [19, 20].

The NCA is a reliable approximation [21] away from very low temperatures where it fails to reproduce the Fermi-liquid behavior in fully screened Kondo systems [22] and where spurious spectral feature appears at the Fermi energy [22, 23]. At typical experimental temperatures NCA is a good choice for this type of calculation because it retains all the electronic structure of the one-electron part of the Hamiltonian while keeping a correct description of the main Kondo features. In fact, the main limitation of our theory rather comes from the use of the customary local or semi-local approximations to DFT. Indeed, DFT calculations on electronic gaps lead to discrepancies of a factor 2 off the experimental gap [24]. This is definitely a big drawback when evaluating Kondo temperatures (T_K) because they depend exponentially on the molecular level value. The Kondo temperature depends on the ratio of the molecular eigenvalue to its broadening, due to the molecular hybridization with the metal substrate. We will use this ratio as

a parameter. Yet, our procedure retains the symmetry and the relative strengths of the one-electron Hamiltonian as given by DFT. A second important approximation of our work is that of the infinite intramolecular Coulomb energy, $U \to \infty$. Extensions of NCA to treat finite U [25, 26, 27] lead to considerable improvement of the T_K. However, since the LDA based electronic structure impedes the calculation of the T_K, the infinite U approximation largely suffices for our purposes.

In NCA, The Kondo physics is modeled by virtual fluctuations of the impurity occupancy. These fluctuations are made possible by coupling the Kondo impurity to the substrate. In principle, NCA can treat all possible configurations. The $U \to \infty$ approximation is admissible, provided that the self-energy contribution due to configurations with two electrons or more is negligible. One can generalize this idea and indeed consider two sets of configurations which differ by the addition of one electron, energetically separated from other configurations by some large value "U" [16]. Hence, with NCA we can treat impurities of increasing complexity, where the physics involved will correspond to virtual fluctuations among configurations differing in electron number by one.

In this way, Roura Bas and Aligia have treated the singlet-triplet quantum transition of an Anderson impurity within NCA [28, 29]. We use a similar approach to describe the configurations of a copper phthalocyanine (CuPc) on Ag (100). On this surface, CuPc captures one electron from the substrate [30] while maintaining a very localized spin on the copper atom at the center of the molecule. Hence, this system is properly characterized by a Hamiltonian describing singlet-triplet transitions. In order to perform our multi-orbital NCA calculations, we first simulate CuPc/Ag(100) with DFT, we transform to a maximally-localized Wannier function (MLWF) basis set [31], and solve the DFT Hamiltonian expressed in this basis set with our multi-orbital NCA code, selecting molecular orbitals that take part in the Kondo physics.

The use of MLWF is mandatory to be able to unambiguously transform the DFT Hamiltonian into an Anderson-like one as we have shown in [31]. This is perhaps the biggest difference with other works using impurity solvers based on DFT calculations [32, 33, 34]. Our approach is thus algorithmic, except for the tuning of the molecular-orbital levels with respect to their hybridization with the substrate since these are quantities where current DFT approaches fail.

In the following section we give more details regarding the implementation and execution of the calculations on CuPc/Ag(100). In section 3, we first show the DFT results and their conversion to the MLWF basis set. The MLWF results permit us to explore the electronic structure that is involved in Kondo physics. We also evaluate the spectral functions for the lowest unoccupied molecular orbital (LUMO) that is actively involved in the generation of Kondo spectral features. Finally, we analyze our results and conclude this work.

2. Method

The NCA is particularly adequate for describing the electronic structure at different energy scales. Our multi-orbital implementation [16] uses the mean-field results of a local density approximation (LDA) calculation, transforms the LDA Hamiltonian into a MLWF basis which permits us to write an Anderson Hamiltonian, $U \to \infty$, while keeping the full multi-configurational aspects of the problem [31]. The NCA is applied on the obtained Anderson Hamiltonian. In this way, the calculated electronic structure contains all molecular+substrate information in the presence of Kondo physics. In this section, we give details on how this is achieved, with special care in the choice of the configurations that will determine the Kondo physics of CuPc on Ag (100).

2.1. Density functional calculations

Density functional calculations of gas phase copper phthalocyanine (CuPc) capture the relevant electronic and geometric properties of the molecule [35]. Briefly, CuPc is a D_{4h} molecule, figure 1, where the d electrons of the central copper atom are split by the ligand field of the surrounding atoms. The ligands capture ~ 2 electrons of the Cu atom rendering the molecule in a magnetic d^9 configuration [35]. The d manifold is split such that the $d_{x^2-y^2}$ orbital is singly occupied (SOMO, the singly occupied molecular orbital). The following empty orbital (LUMO, lowest unoccupied molecular orbital) has π character and double degeneracy, because it constitutes the e_g representation [35] of the point group.

Previous studies using LDA of CuPc on Ag (100) show that the main electronic properties of the adsorbed molecule are retained in the calculation [30]. Here, we take on that work and extract the relevant one-electron physics important for determining the Kondo state.

We have used the SIESTA code [36], relaxed the molecule and first two surface layers to forces below 0.04 eV/Å using the geometry of the reference [30]. The calculations are periodic, using a super-cell containing five layers of 7×7 Ag atoms. This unit cell size is converged for computing electronic structure features of the adsorbed CuPc on Ag(100) [30]. The electronic structure calculations have been done with norm-conserving pseudo-potentials [37] and strictly localized, DZP numerical atom-centered basis set, optimized for this system [30]. The basis sets are build using the method by Anglada *et al.* [38], and we have used the improved noble metal surface description using the basis sets of the reference [39]. The confinement radii (all in Bohr) of s-type first-ζ basis functions were 6.06 for hydrogen, 5.20 (C), 5.64 (N), 5.77 (Cu) and 5.55 (Ag). The confinement radius of the first-ζ extended diffuse orbitals was 7.75. Good agreement with our previous work [30] is thus attained.

The Kohn-Sham Bloch functions were calculated on a Monkhorst-Pack grid $2 \times 2 \times 1$ and transformed to the basis of maximally localized Wannier functions [40, 41, 42] (MLWF). Our method for obtaining MLWF from SIESTA is described in [31].

2.2. Maximally-localized Wannier functions

The main reasons for working with a MLWF basis set are: (*i*) the reduction of the computational problem by projecting the M-dimensional Hilbert space of Kohn-Sham states, where M is the full dimension of the CuPc plus Ag (100) electronic problem, onto a smaller N-dimensional space which faithfully represents [41] the energy bands around the Fermi level taking part in the Kondo effect; (*ii*) the orthogonality of the MLWF basis set that permits us to use standard multi-orbital NCA [16, 22], and (*iii*) the extreme localization of MLWF plus their orthogonality gives us a natural way to partition the problem into impurity and substrate subspaces [31].

Maximally localized Wannier functions have been used in the study of strongly correlated matter (for instance see [43, 44, 45, 46]). In some cases, the spread minimization is skipped and the Kohn-Sham electronic structure is projected directly onto trial orbitals. This strategy has been used in the study of transition metal oxides [47]. In our system, we found that the projection onto trial orbitals gives unreliable results. The disentanglement method [41] can be contrasted with direct selection of certain bands of interest. This is often done in the study of transition metal oxides where bands bear strong orbital character [47, 48]. In the adsorbate problem, the band structure is far more complex, which impedes direct band selection. We conclude that the MLWF are an optimal choice for the problem of a large molecule on a metallic substrate.

For the substrate's MLWF, we choose to describe the $s - p$ bands only. In order to achieve this, the $s - p$ bands of the slab are generated by interstitial Wannier functions, in the same way as the surface state of Cu(111) was achieved in [31]. This is a reasonable selection, as long as Kondo physics is considered, because the d bands start at $\sim$ -3 eV below the Fermi energy. This is away from the relevant region in energy with an energy scale several orders of magnitude larger than the typical Kondo scale. Additionally, d-states are rather localized, presenting small coupling with molecular states. For these two reasons d states can be safely omitted in the description of the substrate electronic structure taking place in the Kondo effect. The choice of the interstitial centers for the MLWF is delicate because CuPc on Ag (100) displays a C_4 symmetry [30] and it is crucial to ensure that MLWF do not reduce the symmetry of the problem. An unexpected problem of the obtention of MLWF for an extended surface is that convergence to MLWF is more difficult as the lateral dimensions of the super-cell are increased. The surface had to be repeatedly tested to achieve a good description of its electronic bands within 2 eV of the Fermi energy.

The molecule's MLWF are obtained jointly with the substrate ones by using the disentanglement method [41]. In order to achieve the clear partitioning between molecule and substrate, the initial set of trial functions consists of 5 d orbitals of the central copper atom (see figure 1), 16 s states for C-H bonds, 32 pz orbitals for every carbon atom, 24 orbitals for the nitrogen atoms and 40 s orbitals for C-C and C-N bonds. This Wannier function description was tested in the two separate systems: the clean Ag (100) surface
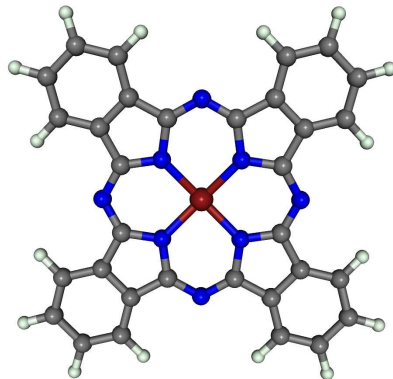
Figure 1. Ball-and-stick scheme of a copper phthalocyanine molecule. The central atom is the copper one, and the rest of atoms are nitrogen, carbon and hydrogen in increasing distance from the central one. The free molecule has a D_{4h} symmetry which is reduced to C_4 upon adsorption on Ag (100) [30].

and the gas phase copper phthalocyanine molecule.

2.2.1. One-particle Hamiltonian In the reference [31], we showed how to obtain an Anderson-like Hamiltonian from a Kohn-Sham Hamiltonian in a MLWF basis set. There, the evaluation of the main quantities of an atomic magnetic impurity in a non-magnetic host was described. Especial emphasis was put on obtaining the intra-atomic Coulomb energy. In the present section, we extend that study to the case of molecules. The Hamiltonian terms have to be expressed in a suitable way to be able to apply the NCA scheme to account for Kondo physics on molecular orbitals.

Thanks to the localization and orthogonality of the MLWF basis, the Wannier-projected Kohn-Sham Hamiltonian can be organized into four blocks

$$\begin{pmatrix} H_{mol} & V' \\ V'^{\dagger} & H_{slab} \end{pmatrix},$$ (1)

where H_{mol} contains matrix elements between molecular Wannier functions, the second block following the diagonal, H_{slab}, refers to Wannier functions of the silver slab, while the off-diagonal blocks, V', involve couplings between molecule and slab.

The eigenstates of H_{mol} are the molecular orbitals now obtained for the MLWF transformed Hamiltonian. As we shall see below, CuPc is a magnetic molecule because one electron is kept in copper's $d_{x^2-y^2}$ orbital. Furthermore, upon adsorption CuPc captures one more electron in the first π-orbital, the doubly degenerated LUMO. Hence, this open-shell structure, when hybridized with the substrate, gives rise to the electron fluctuations of the Kondo effect. These states are singled out of the problem and we define a special subspace for them, $\mathcal{H}_{imp}$, the "impurity" subspace. The rest of states is lumped together into the substrate's subspace, $\mathcal{H}_{subs}$.

Hence, we first apply to (1) a unitary transformation that diagonalizes H_{mol} and leaves H_{slab} untouched. In this way, we obtain the molecular orbitals of the molecular

part of the Hamiltonian, so that the first block of (1) becomes diagonal. Explicitly,

$$
\begin{pmatrix}
TH_{mol}T^{\dagger} & TV' \\
(TV')^{\dagger} & H_{slab}
\end{pmatrix}.
\tag{2}
$$

The unitary matrix T defines the transformation from MLWF of the molecule to molecular orbitals. The second step is to choose the molecular orbitals that play a role in the Kondo effect. These orbitals are placed in the first rows and columns of (2) and define the subspace $\mathscr{H}_{imp}$.

After this rearrangement, the matrix of the Wannier-projected Kohn-Sham Hamiltonian reads

$$
\begin{pmatrix}
\begin{array}{c|c}
H_{imp} & V \\
\hline
V^{\dagger} & H_{subs}
\end{array}
\end{pmatrix}
\tag{3}
$$

where the first block is diagonal and contains selected eigenenergies of H_{mol}, the block H_{subs} contains Hamiltonian matrix elements in $\mathscr{H}_{subs}$ and the block V contains couplings between states in $\mathscr{H}_{imp}$ and $\mathscr{H}_{subs}$. The molecular orbitals that do not directly intervene in the Kondo effect are included in the substrate. Hence, the full mean-field structure of the DFT calculation is preserved within the inner window of the MLWF transformation which is 2 eV around the Fermi energy in the present calculation.

In the present case, the obtention of an Anderson-like Hamiltonian is facilitated by the small values of the intrinsic U term in LDA. As shown in [31], one can extract the intrinsic U term when writing the full Kohn-Sham Hamiltonian in a Wannier-basis set. In that reference, the Co-atom impurity had values of U around 1 eV. For the present method to work, one should subtract the intrinsic U term such as is done in the LDA+U method [49, 50] or in recent parameterizations of model Hamiltonians [51]. Anisimov and coworkers show that this intrinsic U term is related to the Hund's rule exchange and, thus, is much smaller than the actual Coulomb U values. This is particularly true in the case of molecules. In the case of CuPc, we have evaluated the intrinsic U-term to be ~ 30 meV, and hence negligible in front of the molecular level values and hybridization function.

2.2.2.   *Ab-initio calculation of a hybridization function*   The hybridization function has a fundamental role in the impurity physics [52]. It is of uttermost importance to do accurate evaluations of this function for numerical applications. In order to achieve this, we diagonalize H_{subs}, (3), obtaining Bloch states $|\mathbf{k}n\rangle$ and Bloch energies $\epsilon_{\mathbf{k}n}$, n is the band index and $\mathbf{k}$ is from the discretized Brillouin zone with $50 \times 50 \times 1$ k-points. Convergency on $\mathbf{k}$-points was checked by a four-fold increase of the $\mathbf{k}$-point sampling. The couplings V of (3) are transformed to the $|\mathbf{k}n\rangle$ basis accordingly; we label them $V_{\mathbf{k}n,m}$, where m indexes states in $\mathscr{H}_{imp}$. After these manipulations, we can calculate

$$
\Gamma_{mm'}(\omega) = \sum_{\mathbf{k}n} V^{*}_{\mathbf{k}n,m} V_{\mathbf{k}n,m'} \delta(\omega - \epsilon_{\mathbf{k}n})
\tag{4}
$$

from the one-particle Hamiltonian (3). It is a matrix in $\mathscr{H}_{imp}$.

We emphasize that the Hamiltonian (3) is obtained by projecting the Kohn-Sham electronic structure onto a set of N MLWF. The smaller N-dimensional subspace spanned by MLWF is designed in order to represent the selected energy bands around the Fermi level, with the same level of accuracy as the original bands of the M-dimensional space of Kohn-Sham states. The total number of Wannier functions N is the sum of the MLWF of the molecule and of the substrate. The Wannier description has been tested in separate CuPc and Ag(100) systems. M usually means the highest band output from the *ab-initio* calculation. Interestingly, we found that it is very important to verify the *convergence* in M. Inclusion of bands with energy of even tens of eV above the Fermi level is vital and preconditions the correct projection onto the Wannier space. As a consequence, the important value of $\Gamma_{mm}(\omega)$ at the Fermi level turns incorrect if M is too small. In the present case, convergence was attained for $N = 705$ and $M = 3000$.

Formally, (3) becomes the one-particle part of the Anderson Hamiltonian on bringing H_{subs} to a diagonal form. Although the procedure we have just introduced is straightforward and essentially algorithmic, it is not correct in principle, because the on-site energies of molecular orbitals in H_{imp} contain certain part of the Coulomb energy that is included in the mean-field-like LDA framework. Furthermore, the inadequacy of Kohn-Sham energies of orbitals lying close to the Fermi level is well known. In our approach, H_{imp} is replaced by a parameterized model Hamiltonian with many-body interactions. This is a natural step, in view of the fact that we would not have to deal with Hamiltonian partitions like in (3) if standard *ab-initio* calculations included the relevant many-body interactions correctly.

2.3. Impurity electronic configurations

In this work, the one-particle Hamiltonian H_{imp} is replaced by a Hamiltonian $\hat{h}$ with many-body interactions. This subsection discusses the physical grounds on which $\hat{h}$ is designed.

The experimental analysis on the Kondo features in CuPc/Ag(100) [13] indicates that the two-fold degenerate e_g LUMO has the main role in Kondo fluctuations. However, DFT calculations[30] show that the spin in the SOMO orbital is not quenched by charge transfer from the molecule. Hence, the observed Kondo resonance is interpreted [13] as due to a spin $S = 1$ of the molecule, formed by an electron in LUMO and one electron in SOMO. The LUMO electron is captured from the substrate upon adsorption.

We adopt this interpretation and model the molecule as an impurity with a two-electron $S = 1$ ground state. Furthermore, the lifetime of the SOMO will be assumed an order of magnitude longer than the LUMO's, as will be confirmed by *ab-initio* calculation in section 3.1.2.

The electron in the SOMO will be represented by a local magnetic moment which interacts via exchange with the hybridized LUMO. The multi-orbital structure of the
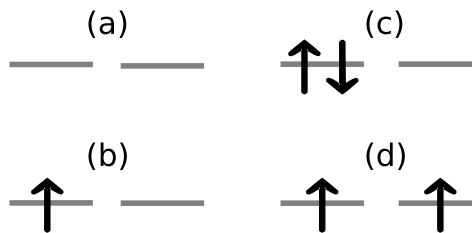
Figure 2. Considered electronic configurations for the two-fold LUMO (e_g): (a) The empty orbital (denoted by e_g^0), (b) singly occupied orbital e_g^1, (c) doubly occupied configuration e_g^2, (d) doubly occupied configuration e_g^{11}.

problem appears in the twofold degeneracy of the LUMO. The configurations that we will study are then the ones coming from the filling of the LUMO, figure 2.

We choose the relevant configurations by estimating their energetic accessibility in the charge fluctuation process. Then, the relevant parameters determining the electronic configuration are: the LUMO on-site energy ϵ_L and the charging energy U. The lowest-energy molecular configuration for the adsorbed molecule is singly occupied, as suggested by DFT calculations [30]. We can estimate the free-molecule U by evaluating the energies of the neutral (E_0), singly (E_I) and doubly (E_{II}) negatively charged molecule. Assuming a simple impurity Hamiltonian, then the affinity is given by

$$E_I - E_0 = \epsilon_L \tag{5}$$

and the second affinity by

$$E_{II} - E_I = 2\epsilon_L + U \tag{6}$$

from these equations and the total energy calculations for the free molecular species we obtain that $U = 2.08$ eV. However, U is substantially screened on the metallic surface. A constrained DFT calculation for π-systems on silver surfaces leads to a reduction of U to values between 0.5 and 1.0 eV [53]. In the present case we take $\epsilon_L = -0.35$ eV (see section 3.2), which leads to $|\epsilon_L| < U$ and the doubly occupied configurations e_g^2, e_g^{11}, figure 2 (c,d), are higher in energy than the neutral one, figure 2 (a). Hence, we will consider $e_g^1 - e_g^0$ fluctuations.

Hence, the impurity Hamiltonian contains the eigenvalues of the two LUMO as given by the diagonalization of the MLWF Hamiltonian (2), plus the exchange interaction I with the spin of the SOMO:

$$\hat{h} = \epsilon_L \sum_{a=1,2} \sum_{\sigma} |a\sigma\rangle\langle a\sigma| - I\mathbf{S}_1 \cdot \mathbf{S}_2. \tag{7}$$

We introduce Hubbard operators which automatically restrict the LUMO occupancy to zero or one. The sums are over spin and orbital degrees of freedom, the latter indexed by a. The second term in the Hamiltonian is the direct exchange interaction involving the spin $\mathbf{S}_2$ of the SOMO and the spin operator of the LUMO expressed through Pauli

matrices $\boldsymbol{\tau}$ as

$$\mathbf{S}_1 = \sum_{\sigma\sigma'} \left(\frac{\boldsymbol{\tau}_{\sigma'\sigma}}{2} \right) \sum_{a=1,2} |a\sigma'\rangle\langle a\sigma| .$$

If $I = 0$ the Schrieffer-Wolff projection of the model onto the e_g^1 manifold leads to a SU(4) Coqblin-Schrieffer model [54]. The evolution of spectral features with I leads to a quantum phase transition of the singlet-triplet impurity problem, that has recently received much attention experimentally [55] and theoretically [28, 29]. Here, we will study three cases: $I < 0$, $I = 0$ and $I > 0$.

2.4. Multi-orbital non-crossing approximation

The above impurity Hamiltonian (7) commutes both with the LUMO occupancy operator, $n_a = \sum_\sigma |a\sigma\rangle\langle a\sigma|$, and the total spin operator $\mathbf{S} = \mathbf{S}_1 + \mathbf{S}_2$ showing that it properly describes the molecular properties. Due to the hybridization with the substrate, the molecule will exchange electrons. Here, we assume just fluctuations between the two above configurations, figure 2 (a) and (b) plus the fluctuations of the SOMO spin, as included in the definition of $\hat{h}$.

The full Anderson-like Hamiltonian reads

$$\hat{H} = \hat{h} + \sum_{\mathbf{k}\sigma} \epsilon_{\mathbf{k}\sigma} c_{\mathbf{k}\sigma}^\dagger c_{\mathbf{k}\sigma} + \hat{V} \tag{8a}$$

$$\hat{V} = \sum_{\mathbf{k}\sigma} \sum_{a} \left(V_{\mathbf{k}\sigma,a} c_{\mathbf{k}\sigma}^\dagger |0\rangle\langle a\sigma| + V_{\mathbf{k}\sigma,a}^* |a\sigma\rangle\langle 0| c_{\mathbf{k}\sigma} \right) . \tag{8b}$$

The hybridization part $\hat{V}$ and the impurity Hamiltonian $\hat{h}$ are written with Hubbard operators which change the state of LUMO from empty to occupied or vice versa. Substrate electrons are described by fermionic operators $c_{\mathbf{k}\sigma}$ and energies $\epsilon_{\mathbf{k}\sigma}$. For the sake of brevity, all substrate-electronic degrees of freedom are encapsulated in the $\mathbf{k}$ symbol. The band index will be introduced when necessary.

Let $\hat{H}_0 = \hat{H} - \hat{V}$. Following Bickers [18], we write down a resolvent operator of the impurity

$$\hat{R}(z) = \frac{1}{Z^{subs}} \sum_{\Omega} e^{-\beta E_\Omega} \langle\Omega| \frac{1}{z - (\hat{H}_0 - E_\Omega) - \hat{V}} |\Omega\rangle$$

as a result of averaging over eigenstates $|\Omega\rangle$ of the non-interacting substrate with energies E_Ω. The substrate partition function is denoted by Z^{subs}. Since $\hat{R}(z)$ does not mix different occupancies, it can be written as a block matrix

$$\hat{R}(z) = \begin{pmatrix} \hat{R}_1(z) & 0 \\ 0 & \hat{R}_2(z) \end{pmatrix} ,$$

where $\hat{R}_1(z)$ refers to one-electron occupancy (ie LUMO empty) and $\hat{R}_2(z)$ acts on two electron occupancies of the impurity.

These quantities are calculated via self-energies defined by

$$\hat{R}_1(z) = \frac{1}{z - \hat{h}|_{N=1} - \hat{\Sigma}_1(z)}$$

$$\hat{R}_2(z) = \frac{1}{z - \hat{h}|_{N=2} - \hat{\Sigma}_2(z)}.$$

Following Kuramoto [16], we introduce basis states labeled by α for the configurations with one electron and β for the two-electron configurations. In the *Non-Crossing Approximation* the self-energies for the fixed occupations are given by all diagrams without crossings of substrate electron lines,

$$\Sigma_{1\alpha'\alpha}(\omega) = \sum_{\beta\beta'} \sum_{\mathbf{k}\sigma} f(\epsilon_{\mathbf{k}\sigma}) V_{\mathbf{k}\sigma}(\alpha'|\beta')$$

$$\times R_{2\beta'\beta}(\omega + \epsilon_{\mathbf{k}\sigma}) V_{\mathbf{k}\sigma}(\beta|\alpha)$$

$$\Sigma_{2\beta'\beta}(\omega) = \sum_{\alpha'\alpha} \sum_{\mathbf{k}\sigma} f(-\epsilon_{\mathbf{k}\sigma}) V_{\mathbf{k}\sigma}(\beta'|\alpha')$$

$$\times R_{1\alpha'\alpha}(\omega - \epsilon_{\mathbf{k}\sigma}) V_{\mathbf{k}\sigma}(\alpha|\beta).$$

The hybridization vertex $V_{\mathbf{k}\sigma}(\alpha|\beta)$ comes when emitting an electron from LUMO to the band state $\mathbf{k}\sigma$ which is accompanied by impurity transition from β to the state with label α. Similarly, $V_{\mathbf{k}\sigma}(\beta|\alpha)$ is brought about when annihilating a one-electron state α of the impurity and creating a two electron state by absorbing a substrate electron. Explicitly,

$$V_{\mathbf{k}\sigma}(\alpha|\beta) = \langle\alpha| c_{\mathbf{k}\sigma} \hat{V} |\beta\rangle \tag{9a}$$

$$V_{\mathbf{k}\sigma}(\beta|\alpha) = \langle\beta| \hat{V} c^{\dagger}_{\mathbf{k}\sigma} |\alpha\rangle. \tag{9b}$$

It is convenient to re-express the fixed-occupation self-energies (also called bosonic and fermionic self-energies in slave-boson approaches [17, 22, 29]) in terms of a hybridization function that is directly related to the level broadening of the impurity configurations

$$\Gamma(\alpha'\beta|\beta'\alpha;\ \omega) = \sum_{\mathbf{k}\sigma} V_{\mathbf{k}\sigma}(\alpha'|\beta') V_{\mathbf{k}\sigma}(\beta|\alpha) \delta(\omega - \epsilon_{\mathbf{k}\sigma}). \tag{10}$$

Please, notice that we have not included π or 2π factors as sometimes is done in the literature. In order to evaluate lifetimes a factor 2π will be added to the diagonal terms of the hybridization function (10).

We can now represent the fixed-occupation self-energies in the form

$$\Sigma_{1\alpha'\alpha}(\omega) = \sum_{\beta\beta'} \int f(\omega') \Gamma(\alpha'\beta|\beta'\alpha;\omega') R_{2\beta'\beta}(\omega + \omega') \mathrm{d}\omega' \tag{11a}$$

$$\Sigma_{2\beta\beta'}(\omega) = \sum_{\alpha'\alpha} \int f(-\omega') \Gamma(\alpha'\beta|\beta'\alpha;\omega') R_{1\alpha\alpha'}(\omega - \omega') \mathrm{d}\omega'. \tag{11b}$$

This permits us to efficiently perform all computations using fast Fourier transforms.

Let us write $\beta = (a, S, S^z)$, where $a = 1, 2$ indexes the two orbitals of LUMO, S the total spin and S^z one of its components. Similarly, α will denote the projection of the spin of SOMO on the z-axis, the only degree of freedom of the one-electron configurations.

In the present case, the substrate is non-magnetic, $\epsilon_{\mathbf{k}\sigma}$ and $V_{\mathbf{k}\sigma,a}$ do not depend on the electron spin, σ, and the expression for the hybridization factorizes into spin and orbital parts (see Appendix). This considerably simplifies the equations (11). Introducing

$$R_1(\omega) = [\omega - \Sigma_1(\omega)]^{-1} \tag{12a}$$

$$\left[R_2^{S=0}(\omega)\right]_{aa'}^{-1} = (\omega - \epsilon_a + \frac{3}{4}I)\delta_{aa'} - \Sigma_{2,aa'}(\omega) \tag{12b}$$

$$\left[R_2^{S=1}(\omega)\right]_{aa'}^{-1} = (\omega - \epsilon_a - \frac{1}{4}I)\delta_{aa'} - \Sigma_{2,aa'}(\omega) \tag{12c}$$

and defining the orbital part of the hybridization function by (see (A.1))

$$\Gamma_{aa'}(\omega) = \sum_{\mathbf{k}} V_{\mathbf{k}a'}^* V_{\mathbf{k}a} \delta(\omega - \epsilon_{\mathbf{k}}), \tag{13}$$

we can write

$$\Sigma_1(\omega) = \sum_{aa'} \int f(\omega')\Gamma_{aa'}(\omega') \times$$
$$\left[\frac{3}{2}R_{2,a'a}^{S=1}(\omega + \omega') + \frac{1}{2}R_{2,a'a}^{S=0}(\omega + \omega')\right] \mathrm{d}\omega' \tag{14a}$$

$$\Sigma_{2,aa'}(\omega) = \int f(-\omega')\Gamma_{aa'}(\omega')R_1(\omega - \omega')\mathrm{d}\omega'. \tag{14b}$$

The resolvent for the two-electron configurations $R_{2,aa'}^{S}$ now depends on the total spin and is a matrix in the orbital space. The equations (12,14) constitute a self-consistent system.

The main quantity of interest, the Green's function of LUMO, will be calculated from the general time-ordered correlation function of Hubbard operators, defined through the thermal average

$$G(\alpha'\beta', \tau|\beta\alpha, 0) = -T_\tau \left\langle e^{\tau H} |\alpha'\rangle\langle\beta'| e^{-\tau H} |\beta\rangle\langle\alpha| \right\rangle. \tag{15}$$

Starting from the latter expression, we average over the singly-occupied configurations $\alpha\alpha'$ and take the Fourier transform [16] to obtain the Green's function of LUMO for the given spin multiplet

$$G_{aa'}^{S}(\omega) = \frac{1}{Z_i} \int \left[R_{2,aa'}^{S}(\omega + \epsilon)A_1(\epsilon) - \right. \tag{16}$$

$$\left. -A_{2,aa'}^{S}(\epsilon)R_1(\epsilon - \omega)\right]e^{-\beta\epsilon}\mathrm{d}\epsilon. \tag{17}$$

The quantities $A_{2,aa'}$ and A_1 are the spectral functions of the resolvents and Z_i is the impurity partition function. We follow Kuramoto [16] and use defect propagators in the numerical implementation of (17), see Appendix.

The spectral function of LUMO is calculated by tracing over orbital and spin degrees of freedom,

$$A(\omega) = -\frac{1}{\pi}\Im m \sum_a \left[G_{aa}^{S=0}(\omega) + 3\, G_{aa}^{S=1}(\omega) \right]. \tag{18}$$

We see that the general Green's function (15) factorizes into channels of the total spin of an incoming electron (hole) and the molecule (17). This fact has been used to model magnetic inelastic effects induced by the STM [56, 57, 58].

3. Results: Kondo Physics of CuPc on Ag (100)

Full detail on the adsorption of CuPc on Ag (100) is given in other publications [30, 59]. Here, we build on those results and apply our methodology to obtain the electronic structure in presence of the Kondo effect. First, we build the Anderson-like Hamiltonian following the recipes of section 2.2.1 and next, we solve the multi-orbital NCA equations, section 2.4, presenting the spectral function or PDOS onto CuPc doubly degenerated LUMO. Special care is given to the evaluation and presentation of the hybridization function, $\Gamma_{mm'}(\omega)$, of section 2.2.2 because most of the relevant Kondo physics is associated with the symmetry and values of this function.

3.1. Hamiltonian for CuPc on Ag (100)

3.1.1. Molecular orbitals Thanks to the partitioning made possible by the MLWF basis, we can extract the molecular Hamiltonian H_{mol} (1) computed from the LDA calculation of CuPc on Ag (100) [30, 59]. Table 1 presents eigenenergies of H_{mol} the molecular orbitals close to the substrate's Fermi level. The orbitals are then closely related to the gas-phase CuPc ones and hence, we denote them by SOMO, LUMO and highest occupied molecular orbital (HOMO) labels. For comparison, the results for the LDA SIESTA calculation of the gas-phase molecule of the same molecular geometry are also given. The MLWF qualitatively reproduce the gas phase molecular levels. We emphasize that the ϵ (MLWF) refer to molecular orbitals screened by the metal but without direct hybridization and the ϵ (SIESTA) are for a true gas-phase molecule without any screening or coupling with an external metal.

Figure 3 shows the PDOS onto these four molecular orbitals. The calculation is performed for the LDA k-point grid $(2 \times 2 \times 1)$ which is clearly insufficient to account for the continuum character of the substrate electronic states. Hence, the peaks have been slightly broadened using a Gaussian broadening of 50 meV. Despite the qualitative character of this figure, much information can be gleaned from it. The difference in widths between SOMO on one hand and LUMO and HOMO on the other hand is substantial. The SOMO peak basically presents the numerical width, and is a featureless
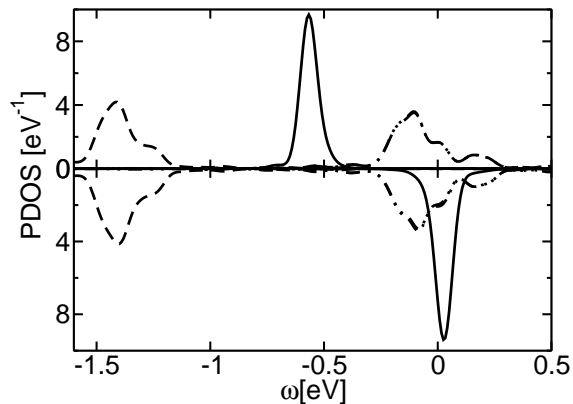
Figure 3. Density of states projected onto molecular orbitals (PDOS). The projection onto the SOMO is given by bold lines, onto the HOMO by dashed lines and onto the LUMO by dash-dotted lines. Energies are with respect to the Fermi energy. Majority spin is shown in the upper panel and minority in the lower one. The PDOS are convoluted with a 50-meV Gaussian.

peak, while the LUMO shows oscillations and spreads over several hundreds of meV. Then, the latter orbitals hybridize more strongly with the substrate. From this figure we can conclude that while the LUMO width is in the range of a few hundreds of meV, the SOMO is significantly less. This is in agreement with the move involved calculations of the hybridization function that we present in the next section.

The PDOS are in excellent agreement with the PDOS on molecular orbitals from DFT results [59]. Both the eigen-energies and the PDOS give support to our method of transforming the DFT Hamiltonian to a MLWF and selecting the impurity Hamiltonian using (3).

Table 1. Eigenenergies of the molecular orbitals for the impurity Hamiltonian evaluated with MLWF using (2), compared with the gas phase LDA calculation using SIESTA, for the same geometry of the CuPc molecule. All energies in the third column were shifted, so that the energies of SOMO ($\downarrow$) coincide. Energies of the second LUMO state are in parenthesis. The comparison is only indicative that the MLWF capture the molecular properties since the two calculations are performed for different systems: the MLWF refers to molecular orbitals screened by the metal but without direct hybridization and the SIESTA column is for a true gas-phase molecule without any screening or coupling with an external metal.

	ϵ (MLWF) [eV]	ϵ (SIESTA) [eV]
HOMO ($\uparrow$)	-1.110	-0.888
HOMO ($\downarrow$)	-1.112	-0.890
SOMO ($\uparrow$)	-0.549	-0.714
SOMO ($\downarrow$)	0.040	0.040
LUMO ($\uparrow$)	0.185 (0.190)	0.496 (0.498)
LUMO ($\downarrow$)	0.211 (0.216)	0.520 (0.522)

It is difficult to conclude on the actual occupancies from the PDOS. Indeed, the

PDOS numerical broadening thwarts any precise calculation of orbital occupancies, and the definition itself of occupancy of a molecular orbital in a chemisorbed system is somewhat arbitrary. As we show in the next section, the actual peak width of SOMO is negligible; the SOMO then remains singly occupied as in the gas phase. The LUMO peaks in figure 3 cross the Fermi level, hence these orbitals capture charge from the substrate. The LUMO are then the only orbitals that participate in charge transfer from the surface.

3.1.2. Hybridization function The lack of continuum in the PDOS calculation is cured in the calculation of the hybridization function (4). Thanks to the smaller size of the MLWF Hamiltonian (3), we can now find the Bloch functions for a very dense k-point grid.

The off-diagonal parts of $\Gamma_{mm'}(\omega)$ are very small (< 1 meV). This is a very strong result that shows that the substrate does not mix the different molecular orbitals among themselves. Hence, every molecular orbital defines an electronic channel of the system.

The diagonal elements for SOMO and LUMO orbitals are presented in figure 4, along with the density of states of the substrate. The three curves are very similar in shape. By comparing the hybridization functions with the substrate DOS, we notice that the hybridization function grows more slowly than the DOS as the electron energy increases. This is an effect due to the couplings, V, between the molecular orbitals and the substrate electronic structure. However, at higher energy, it is the DOS that controls the behavior of the hybridization function with energy. Figure 4 shows that the SOMO width has to be multiplied by 20 to be comparable to the LUMO one. The SOMO orbital has then a very small mixing with the substrate as compared to the LUMO. Finally, in the $U = 0$ picture, the FWHM for the LUMO is $2\pi\Gamma_{aa}(\omega = \epsilon_L) = 440$ meV and is comparable to the FWHM of the PDOS peak, figure 3, obtained with an insufficient k-point sampling.

We have also evaluated the hybridization function of the LUMO with d orbitals by preparing a Wannier basis-set with d orbitals. In the region of interest here (some 2 eV about the Fermi energy), this hybridization is strictly zero due to the lack of d states at these energies. However, when resonant with Ag d-band (3 eV below the Fermi energy), the hybridization function becomes larger than the corresponding values for the sp Wannier functions. At 4 eV below the Fermi energy, the d-electron hybridization has maximum of 0.032 eV, while the sp one is 0.035 eV. The consequence of this is that the spectral function at -4 eV will not be just a simple Lorentzian tail. However, the LUMO orbital is some hundreds of meV away from the Fermi energy, and the effect of the d-band contribution to the overall shape of the LUMO spectral function is negligible both for Kondo physics and for the one-electron spectral shape.

Finally, we comment on the problem of broken spin symmetry in DFT. Spin-polarized LDA implies two subsystems: minority and majority spin. This in turn says that we have two sets of Wannier functions, two distinct substrates, hybridization functions, etc. The main effect of breaking the spin invariance in our DFT calculation
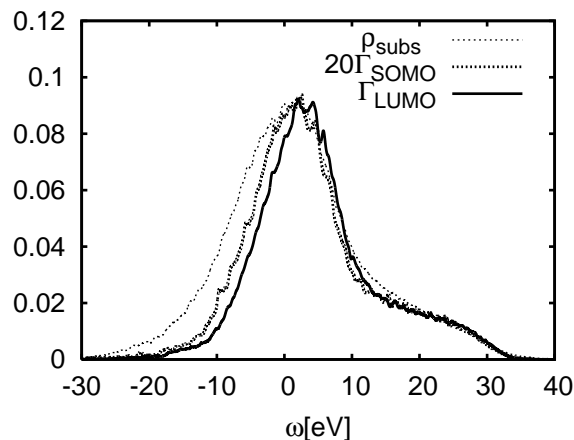
Figure 4. Diagonal elements of the hybridization function matrix (in eV) as a function of the electron energy, ω, with respect to the Fermi level. Only the LUMO and the SOMO (note the factor 20) are considered. For comparison, the substrate-projected density of states is given in arbitrary units. The delta function of (4) has been replaced by a 5-meV wide Gaussian; the k-point sampling is $50 \times 50 \times 1$.

is that the SOMO occupancy is $n_{SOMO} \approx 1$. As a secondary effect, the substrate and molecule become slightly spin-polarized as well. However, this effect is perturbational [14] and is not an intrinsic property of the bare substrate and impurity of the Anderson model. In what follows we drop the minority spin data of the hybridization function and restore the spin symmetry.

3.2. Multi-orbital NCA results

Our LDA calculations yield a hybridization function for the SOMO, Γ_S, ten times smaller than the one for the LUMO levels. From these values we obtain $\Gamma_S \approx 4.5$ meV. We use the standard expression for the Kondo temperature [60]

$$T_{K,S} = D \exp\left(-\frac{|\epsilon_S|}{2\Gamma_S}\right) \tag{19}$$

and take the *ab-initio* value for the on-site energy from the table 1. The bandwidth is 2D, where a rectangular DOS is typically assumed. Here we have taken D as 10 eV because the DOS of Fig. 3 integrates to 703 states, while the calculated DOS at the Fermi energy is 32.28 eV^{-1}. Hence 2D=703/32.28=21.8 eV, and D turns out roughly 10 eV. We get $T_{K,S}$ of the range 10^{-26} eV. Thus, the energy scale that would correspond to a Kondo effect on the SOMO orbital (without exchange coupling to LUMO) is unobservable.

These arguments show that the Kondo coupling in this system is indeed given by virtual charge fluctuations of the two-fold degenerate LUMO. Hence, we are dealing with the impurity problem described in section 2.3, for which we can calculate the spectral function according to the section 2.4.

However, the on-site energies of LUMO in (7) as given by their LDA values in the table 1 lie very close to the Fermi level, which would correspond to a fluctuating valence
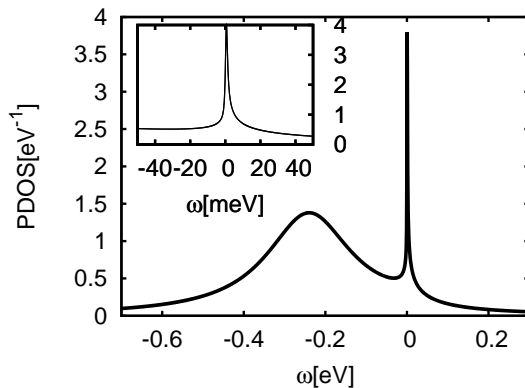
Figure 5. LUMO spectral function for the $I = 0$ case. The wide peak corresponds to a charge excitation and the narrow peak is the Kondo peak (shown also in the inset).

regime. That has not been observed in the experiment [13]. This is related to the fact that the LDA energies of LUMO do not reflect the considerable Coulomb repulsion in their spin splitting. We fix these deficiencies by rescaling the $\epsilon_L/\Gamma_{aa}(\omega)$ ratio in order to achieve a $SU(4)$ Kondo temperature, $T_{K,L} = D \exp\left(-|\epsilon_L|/4\Gamma_{aa}\right)$, of $\sim$20 K as observed in the measurements [13]. The results presented in this section are calculated with $\epsilon_L = -0.35$ eV and $\Gamma_{aa}(\epsilon_L)$ rescaled to 0.01 eV.

Below $T_{K,L}$, the model exhibits a rich variety of physics as the value of I changes. For $I \geq 0$ but smaller than the Kondo temperature $T_{K,L}$, the SOMO is effectively decoupled from the LUMO and we recover the case of two degenerated LUMO on the same footing as the electron spin: we have an $SU(4)$ system as described above. For negative I, $|I| \lesssim T_{K,L}$, the SOMO becomes screened by a two-stage Kondo effect at very low temperatures. For positive and large $I \gg \Gamma_{aa}, T_{K,L}$, the Kondo physics is that of the under-screened Kondo effect, because of the $S = 1$ molecular ground state. Hence, the model will show singular Fermi liquid characteristics [61, 62, 63] in the low-energy domain. Finally, in the limit $I \to -\infty$, we obtain a spin zero molecule with orbital pseudo-spin, which is over-screened by two substrate channels. The cross-over temperature is, however, exponentially smaller than $T_{K,L}$, due to the reduced degeneracy. Here we present NCA spectral functions in the $I = 0$ case and in the intermediate regimes $\Gamma_{aa} > |I| > T_{K,L}$ which are dominated by inelastic spin transitions.

Figure 5 shows the spectral function of LUMO at $T = 7K$ when the exchange interaction between SOMO and LUMO is turned off, $I = 0$. The ground state of $\hat{h}$ is fourfold degenerate in this case. Since each of the two orbitals of LUMO defines an independent scattering channel in the substrate (ie $\Gamma_{aa'}(\omega)$ is diagonal), the LUMO is subject to a $SU(4)$ Kondo effect. The spectral function shows a broad charge-excitation peak of the FWHM given by $4 \cdot 2\pi\Gamma_{LL}(\epsilon_L)$ and a narrow Kondo peak.

When the SOMO and LUMO spins are subject to a ferromagnetic interaction ($I > 0$) the ground state of the molecule without couplings to the substrate is an orbitally degenerate $S = 1$. The excited state is a $S = 0$ orbital doublet. Now, two
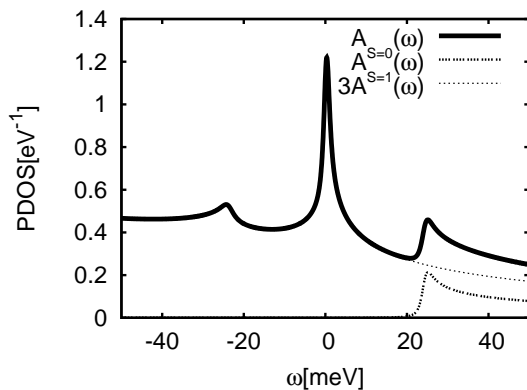
Figure 6. LUMO spectral function for $I = 25$ meV (bold line). The spin zero and spin one channel contributions are presented. The positive-energy satellite corresponds to injection of one electron in the excited electronic structure of the system: the spin zero channel. The negative-energy peak corresponds to removing one electron from the molecular ground state in the $S = 1$ channel.

satellites develop at $\pm I$ from the Kondo peak, figure 6. These satellites are inelastic replicas of the Kondo peak since the spin excitation energy is exactly I. Decomposition into spin channels yields that the Stokes $(+I)$ satellite is in the $S = 0$ channel, while the anti-Stokes peak as well as the Kondo peak are in the $S = 1$ channel. This result can be understood by recalling the meaning of the spectral function. The spectral function at $T = 0$ yields the probability density to inject one electron in the system when $\omega > 0$ or to inject a hole when $\omega < 0$. Hence, the positive energy satellite corresponds to an excited Kondo effect triggered by the injection of an electron to the $S = 0$ state, which is an excited state of $\hat{h}$. Similar results have been found by Roura Bas and Aligia [28, 29].

When the interaction is anti-ferromagnetic $(I < 0)$, the ground state of $\hat{h}$ is an orbital doublet and is followed by six excited states of spin one. A noteworthy feature of the spectral function are the steps typical for an inelastic spin-flip transition (see for example [56, 57] and references therein). The inelastic steps enhanced by Kondo effect have already been explored in the case of singlet-triplet transitions in nanotubes [64]. The spin channel analysis yields that the Stokes peak is now $S = 1$ which again can be rationalized by noticing that it corresponds to injecting an electron in an excited $S = 1$ state and the transition is enhanced by an excited Kondo effect. By the same token, the anti-Stokes peak is $S = 0$ since a hole is created in this channel.

The spectral function, figure 7, shows a small peak on the Fermi level. This peak cannot correspond to a spin-flip Kondo effect. The orbital Kondo resonance is ruled out by its exponentially suppressed energy scale $\propto \exp{(-|\epsilon_L|/2\Gamma_{aa})}$ as compared to $T_{K,L}$. NCA is known to produce spurious peaks at the Fermi level [15, 23, 18]. The temperature scale at which they appear is given by [60] $T_S = T_{K,L}/5[T_{K,L}/\Gamma_{aa}]^{5/3} = 0.18$ K (strictly valid for $I = 0$ only). All calculations shown here are performed at 7 K, well above the pathology temperature T_S. We conjecture that the zero energy structure is
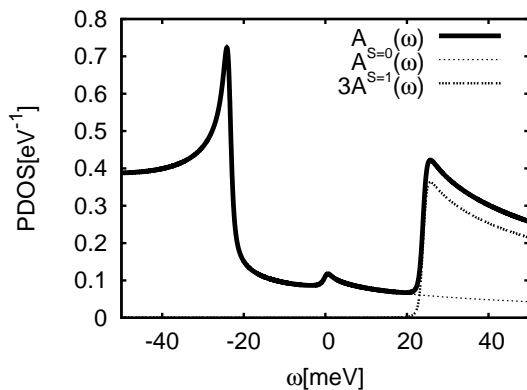
Figure 7. LUMO spectral function for $I = -25$ meV. The spin zero and spin one components are presented. The two excitation steps correspond to inelastic transitions enhanced by the Kondo effect. As in the $S = 1$ case, $I = 25$ meV, the steps belong to a channel with well defined spin. The positive-energy step is given by the spin triplet $(S = 1)$ channel and the low energy peak is due to the $S = 0$ channel.

related to the problems of NCA to reproduce spin-split Kondo peaks, as detailed in [22], p. 25.

A common feature of both $I > 0$ and $I < 0$ spectral functions (figures 6,7) is a certain asymmetry of the Stokes and anti-Stokes peaks. This is caused by asymmetry of the hybridization function with respect to the Fermi energy, or by the $U = \infty$ approximation. We have explicitly verified that the hybridization function has very little effect on the respective heights of both satellites. Indeed, the asymmetry comes from the fact that system is out of the particle-hole symmetry. Then we assign the asymmetry of the satellites to the infinite Coulomb repulsion.

4. Discussion

The evaluated LDA spectral function, figure 3, seems to suggest a fluctuating valence state while a Kondo peak have been experimentally found [13]. Moreover, if we added a strong Coulomb term to the LUMO, the corresponding Anderson Hamiltonian would correspond to an empty-impurity regime according to the scaling theory [65]. For these reasons, we had to rescale the Kondo temperature in our model by shifting the LUMO level and changing the hybridization strength as we showed in the previous section.

These results show that LDA is unreliable to furnish quantitative data. Any *ab-initio* method is bound to failure when trying to estimate the Kondo temperature given the exponential dependence on the main *ab-initio* ingredients: the level position and hybridization. Nevertheless, *ab-initio* calculations can give valuable qualitative input since the correct electronic symmetry addressing both the spin and orbital channels can be directly obtained from DFT. Our analysis of the hybridization function has yielded important information: (*i*) the existence of two well-defined orbital channels originating in the hybridization of the two LUMO with the substrate has been proved because

non-diagonal terms of $\Gamma_{aa'}(\omega)$ are vanishingly small, (*ii*) both LUMO and SOMO are partially charged in the adsorbed system, the LUMO due the sizeable values of Γ_{aa} that leads to charge transfer from the substrate, and the SOMO for the vanishing value of Γ_S that leaves its spin unperturbed. Hence, LDA reveals the orbital $SU(2)$ symmetry associated with LUMO electron and its substrate channels.

The failure of the present LDA calculations to yield a realistic ϵ_L/Γ_{aa} ratio can be traced back to the complete failure in giving the qualitative Kondo physics of the CuPc/Ag(100) system. As we just saw, the PDOS onto Kohn-Sham states predicts the system to be in a mixed-valence regime while the experimental data show it is a Kondo system. This points out at the present failures, namely, the LUMO occupation is poorly accounted for in LDA. Previous works have claimed that LDA is not capable to yield correct hybridization functions, because of the lack of charge discontinuity in the exchange-and-correlation functional [66]. While this is clearly the case in transport calculations, the present hybridization function describes a static situation, where the strength of the coupling to the substrate is evaluated. Furthermore, the hybridization function evaluates the transparency of the barrier between the molecule and the substrate [67]. Hence, we do not think that the hybridization function is affected by the charge discontinuity problem. We think it is rather the electronic configuration that is affected by the charge discontinuity problem yielding wrong occupancies, the alignment of the molecular levels and finally the wrong qualitative picture.

Finally, the cure has already been advanced in the literature by using LDA+U methods [68]. As in the reference [68], U has to be computed for the LUMO orbitals as has been recently realized by an increasing number of groups [53, 68].

It is for these failures of the LDA calculations that the ϵ_L/Γ_{aa} had to be adapted in order to obtain reasonable spectral functions in the section 3.2. In the physically relevant case of the positive SOMO-LUMO exchange coupling of $I = 25$ meV we obtained the experimentally observed three-peak structure in the vicinity of the Fermi level [13].

In spite of the shortcomings stemming from LDA's description of the LUMO shown in this work, we emphasize that the Wannier-based approach is not restricted to the use of LDA functional and can be interfaced to an arbitrary *ab-initio* method which provides a one-particle structure as for example the promising $GW+MLWF$ method [69]. Moreover, Wannier functions allow to take a step beyond the super-cell approach and simulate a true impurity problem (ie a single molecule on a surface) by reconstructing a semi-infinite substrate out of the tight-binding Hamiltonian elements obtained in a super-cell.

5. Conclusion

We have implemented a multi-orbital non-crossing approximation approach based on a standard one-electron *ab-initio* electronic structure. The Kohn-Sham orbitals of a DFT calculation are transformed to a maximally localized Wannier function (MLWF) basis set such that a tight-binding like Hamiltonian is obtained, in view of the locality and

orthogonality of MLWF. This procedure is in principle algorithmic and permits us to have a quantum impurity model from a DFT calculation.

We have applied this methodology to the case of a copper phthalocyanine (CuPc) molecule adsorbed on Ag(100) following existing experimental work [30, 13]. From our DFT calculations we conclude that the two-fold degenerate LUMO captures charge and this can give rise to the Kondo effect. The spin of the SOMO is a spectator because its Kondo energy scale is many orders of magnitude smaller than the one of the LUMO. However, intramolecular exchange interaction between the SOMO and LUMO spin gives rise to a rich singlet-triplet phenomenology that our numerical procedure captures. Our calculations show that two well defined orbital channels emerge in the substrate as dictated by the C_4 point group symmetry. We have further investigated the impurity spectral function in terms of spin channels and we have rationalized the inelastic features of the spectral function for both (spin) singlet and triplet ground states.

This physics has been obtained by rescaling the computed Kondo temperature to fit the experimental one. Indeed, our LDA-based calculation fails to yield a Kondo ground state and rather predicts a fluctuating-valence system. We attribute this error to the lack of charge discontinuity in the LDA exchange-and-correlation functional and suggest that alternative LDA+U methods for the one-electron calculation will improve the agreement with the experimental electronic structure of CuPc on Ag(100).

Appendix A. Non-crossing approximation

Appendix A.1. Spin coefficients for a singlet-triplet impurity

The couplings between α and β (see (9)) are given by the expression

$$V_{\mathbf{k}\sigma}(\alpha'|\beta) = V_{\mathbf{k}\sigma,a} \langle \sigma\alpha|SS^z\rangle$$

with $V_{\mathbf{k}\sigma,a}$ from the Hamiltonian (8) and the braket is a Clebsch-Gordan coefficient. When the substrate is non-magnetic, $\epsilon_{\mathbf{k}\sigma}$ and $V_{\mathbf{k}\sigma,a}$ do not depend on σ and the expression for hybridization intensity (10) factorizes

$$\Gamma(\alpha'a'S'S^{z'}|aSS^z\alpha; \ \omega) = \Gamma_{aa'}(\omega)\gamma_{\alpha'\alpha}(S'S^{z'}|SS^z)$$

into orbital

$$\Gamma_{aa'}(\omega) = \sum_{\mathbf{k}} V_{\mathbf{k}a'}^* V_{\mathbf{k}a}\delta(\omega - \epsilon_{\mathbf{k}}) \tag{A.1}$$

and spin parts

$$\gamma_{\alpha\alpha'}(S'S^{z'}|SS^z) = \sum_{\sigma} \left\langle S'S^{z'}|\sigma\alpha'\right\rangle\!\left\langle\sigma\alpha|SS^z\right\rangle. \tag{A.2}$$

The subsequent identities have proven significant

$$\sum_\alpha \gamma_{\alpha\alpha}(S'S^{z\prime}|SS^z) = \delta_{SS'}\delta_{S^zS^{z\prime}} \tag{A.3}$$

$$\sum_{S^z} \gamma_{\alpha\alpha'}(1S^z|1S^z) = \frac{3}{2}\delta_{\alpha\alpha'} \tag{A.4}$$

$$\gamma_{\alpha\alpha'}(00|00) = \frac{1}{2}\delta_{\alpha\alpha'}. \tag{A.5}$$

The first one is due to completeness (A.2), the second and third can be proven using Wigner *3jm* symbols [70].

With these identities it is easy to show that the following property holds: Let $\hat{R}_1^{test}(\omega)$ and $\hat{R}_2^{test}(\omega)$ be some functions diagonal in the total spin representation, so will the self-energies calculated from NCA (11a), (11b),

$$\Sigma_{1\alpha'\alpha}^{test}(\omega) = \sum_{\beta\beta'} \int f(\omega')\Gamma(\alpha'\beta|\beta'\alpha;\omega')$$
$$\times R_{2\beta'\beta}^{test}(\omega+\omega')\mathrm{d}\omega'$$

$$\Sigma_{2\beta\beta'}^{test}(\omega) = \sum_{\alpha'\alpha} \int f(-\omega')\Gamma(\alpha'\beta|\beta'\alpha;\omega')$$
$$\times R_{1\alpha\alpha'}^{test}(\omega-\omega')\mathrm{d}\omega'.$$

Since we solve the equations of NCA iteratively, starting with resolvents having zero self-energies, we conclude that spin off-diagonal terms of $\hat{R}_{1,2}$ vanish.

Appendix A.2. Evaluation of the physical Green's function using defect propagators

Equation (17) has to be expressed in terms of defect propagators. For convenience we introduce boldface notation for matrices in the orbital space of LUMO, ie $\mathbf{R}_2^S, \mathbf{A}_2^S, \mathbf{\Gamma}, \mathbf{G}^S$ for the resolvent of the two-electron configuration, its spectral density, hybridization function (A.1) and the Green's function of LUMO. The starting expression (17) reads

$$\mathbf{G}^S(\omega) = \frac{1}{Z_i} \int \left[\mathbf{R}_2^S(\omega+\epsilon)A_1(\epsilon) - \right. \tag{A.6}$$

$$\left. -\mathbf{A}_2^S(\epsilon)R_1(\epsilon-\omega)\right]e^{-\beta\epsilon}\mathrm{d}\epsilon. \tag{A.7}$$

We introduce the operator $\mathfrak{P}$, whose effect on an arbitrary matrix function $\mathbf{X}(\omega)$ is given by

$$\mathfrak{P}\mathbf{X}(\omega) = \frac{i}{2\pi Z_i}e^{-\beta\omega}\left[\mathbf{X}(\omega) - \mathbf{X}^\dagger(\omega)\right].$$

By applying $\mathfrak{P}$ on both sides of NCA equations (14) yields a self-consistent system

$$\mathbf{a}_2^S(\omega) = \mathbf{R}_2^S(\omega)\int f(\omega')\mathbf{\Gamma}(\omega')a_1(\omega-\omega')\mathrm{d}\omega'\mathbf{R}_2^{S\dagger}(\omega)$$

$$a_1(\omega) = |A_1(\omega)|^2\frac{1}{2}\sum_{S=0,1}(2S+1)$$

$$\times \int f(-\omega')\mathrm{Tr}\left\{\mathbf{\Gamma}(\omega')\mathbf{a}_2^S(\omega+\omega')\right\}\mathrm{d}\omega'$$

for the defect propagators [23], defined by

$$a_1(\omega) = \mathfrak{P} A_1(\omega) \qquad \text{and} \qquad \mathbf{a}_2(\omega) = \mathfrak{P} \mathbf{A}_2(\omega).$$

When these equations are solved, the Green's function (A.6) can be expressed as

$$\mathbf{G}^S(\omega) = \int \big[\mathbf{R}_2^S(\omega + \epsilon) a_1(\epsilon) - \qquad\qquad (\text{A.8})$$

$$-\mathbf{a}_2^S(\epsilon) R_1(\epsilon - \omega) \big] \mathrm{d}\epsilon. \qquad\qquad (\text{A.9})$$

Acknowledgments

References

[1] J Li, WD Schneider, R Berndt, and B Delley. *Phys. Rev. Lett.*, 80(13):2893–2896, 1998.
[2] V Madhavan, W Chen, T Jamneala, M F Crommie, and N S Wingreen. *Science*, 280(5363), 1998.
[3] N Knorr, M Alexander Schneider, L Diekhöner, P Wahl, and K Kern. *Phys. Rev. Lett.*, 88(9):096804, 2002.
[4] Z Aidi, L Qunxiang, C Lan, X Hongjun, W Weihua, P Shuan, W Bing, X Xudong, Y Jinlong, JG Hou, and Z Qingshi. *Science*, 309(5740), 2005.
[5] V Iancu, A Deshpande, and SW Hla. *Phys. Rev. Lett.*, 97(26):266603, 2006.
[6] L Gao, W Ji, YB Hu, ZH Cheng, ZT Deng, Q Liu, N Jiang, X Lin, W Guo, SX Du, WA Hofer, XC Xie, and HJ Gao. *Phys. Rev. Lett.*, 99(10):106402, 2007.
[7] I Fernández-Torrente, KJ Franke, and JI Pascual. *Phys. Rev. Lett.*, 101(21):217203, 2008.
[8] UGE Perera, HJ Kulik, V Iancu, LGGV Dias da Silva, SE Ulloa, N Marzari, and SW Hla. *Phys. Rev. Lett.*, 105(10):106601, 2010.
[9] D Wegner, R Yamachika, X Zhang, Y Wang, T Baruah, MR Pederson, BM Bartlett, JR Long, and MF Crommie. *Phys. Rev. Lett.*, 103(8):087205, 2009.
[10] P Wahl, L Diekhöner, G Wittich, L Vitali, MA Schneider, and K Kern. *Phys. Rev. Lett.*, 95(16):166601, 2005.
[11] N Néel, J Kröger, R Berndt, TO Wehling, AI Lichtenstein, and MI Katsnelson. *Phys. Rev. Lett.*, 101(26):266803, 2008.
[12] T Komeda et al. submitted.
[13] A Mugarza, C Krull, S Stepanov, G Ceballos, N Lorente, and P Gambardella. Intramolecular resolution and manipulation of spin coupling and non-equilibrium Kondo phenomena in metal-organic complexes. submitted, 2010.
[14] PW Anderson. *Phys. Rev.*, 124(1):41–53, 1961.
[15] N Grewe. *Z. Phys. B*, 53:271, 1983.
[16] Y Kuramoto. *Z. Phys. B*, 53(1):37–52, 1983.
[17] P Coleman. *Phys. Rev. B*, 29(6):3035–3044, 1984.
[18] NE Bickers. *Rev. Mod. Phys.*, 59(4):845–939, 1987.

[19] F Reinert, D Ehm, S Schmidt, G Nicolay, S Hüfner, J Kroha, O Trovarelli, and C Geibel. *Phys. Rev. Lett.*, 87(10):106401, 2001.

[20] Kroha, J and Kirchner, S and Sellier, G and Wölfle, P and Ehm, D and Reinert, F and Hüfner, S and Geibel, C. *Physica E*, 18(1-3):69 – 72, 2003.

[21] FB Anders and N Grewe. *Europhys. Lett.*, 26(7):551–556, 1994.

[22] Kroha, J and Wölfle, P. *J. Phys. Soc. Jpn.*, 74(1):16 – 26, 2005.

[23] Y Kuramoto and H Kojima. *Z. Phys. B*, 57(2):95–105, 1984.

[24] RW Godby, M Schlüter, and LJ Sham. *Phys. Rev. Lett.*, 56(22):2415–2418, 1986.

[25] K Haule, S Kirchner, J Kroha, and P Wölfle. *Phys. Rev. B*, 64(15):155111, 2001.

[26] J Otsuki and Y Kuramoto. *J. Phys. Soc. Jpn.*, 75:064707, 2006.

[27] N Grewe, T Jabben, and S Schmitt. *EPJ B*, 68(1):23–32, 2009.

[28] P Roura Bas and AA Aligia. *Phys. Rev. B*, 80(3):035308, 2009.

[29] P Roura Bas and AA Aligia. *J. Phys.: Condens. Matter*, 22(2):025602, 2010.

[30] A Mugarza, N Lorente, P Ordejón, C Krull, S Stepanow, ML Bocquet, J Fraxedas, G Ceballos, and P Gambardella. *Phys. Rev. Lett.*, 105(11):115702, 2010.

[31] R Korytár, M Pruneda, J Junquera, P Ordejón, and N Lorente. *J. Phys.: Condens. Matter*, 22(38):385601, 2010.

[32] E Gorelov, TO Wehling, AN Rubtsov, MI Katsnelson, and AI Lichtenstein. *Phys. Rev. B*, 80(15):155132, 2009.

[33] D Jacob and G Kotliar. *Phys. Rev. B*, 82(8):085423, 2010.

[34] LGGV Dias da Silva, Murilo L Tiago, SE Ulloa, FA Reboredo, and E Dagotto. *Phys. Rev. B*, 80(15):155443, 2009.

[35] MS Liao and S Scheiner. *J. Chem. Phys.*, 114(13):9780, 2001.

[36] JM Soler, E Artacho, JD Gale, A García, J Junquera, P Ordejón, and D Sánchez-Portal. *J. Phys.: Condens. Matter*, 14:2745, 2002.

[37] N Troullier and JL Martins. *Phys. Rev. B*, 43(3):1993–2006, 1991.

[38] E Anglada, J M. Soler, J Junquera, and E Artacho. *Phys. Rev. B*, 66(20):205101, 2002.

[39] S García-Gil, A García, N Lorente, and P Ordejón. *Phys. Rev. B*, 79(7):075441, 2009.

[40] N Marzari and D Vanderbilt. *Phys. Rev. B*, 56(20):12847–12865, 1997.

[41] I Souza, N Marzari, and D Vanderbilt. *Phys. Rev. B*, 65(3):035109, 2001.

[42] AA Mostofi, JR Yates, YS Lee, I Souza, D Vanderbilt, and N Marzari. *Comput. Phys. Commun.*, 178(9):685 – 699, 2008. www.wannier.org.

[43] H Sakakibara, H Usui, K Kuroki, R Arita, and H Aoki. *Phys. Rev. Lett.*, 105(5):057003, 2010.

[44] H Ikeda, R Arita, and J Kuneš. *Phys. Rev. B*, 81(5):054502, 2010.

[45] F Lechermann, A Georges, A Poteryaev, S Biermann, M Posternak, A Yamasaki, and OK Andersen. *Phys. Rev. B*, 74(12):125120, 2006.

[46] M Karolak, TO Wehling, F Lechermann, and AI Lichtenstein. *J. Phys.: Condens. Matter*, 23(8):085601, 2011.

[47] D Korotin, AV Kozhevnikov, SL Skornyakov, I Leonov, N Binggeli, VI Anisimov, and G Trimarchi. *EPJ B*, 65(1):91–98, 2008.

[48] B Amadon, F Lechermann, A Georges, F Jollet, TO Wehling, and AI Lichtenstein. *Phys. Rev. B*, 77(20):205112, 2008.

[49] VI Anisimov, J Zaanen, and OK Andersen. *Phys. Rev. B*, 44(3):943–954, 1991.

[50] SL Dudarev, G A Botton, SY Savrasov, CJ Humphreys, and AP Sutton. *Phys. Rev. B*, 57(3):1505–1509, 1998.

[51] D Jacob and G Kotliar. *Phys. Rev. B*, 82(8):085423, 2010.

[52] G Kotliar, SY Savrasov, K Haule, VS Oudovenko, O Parcollet, and CA Marianetti. *Rev. Mod. Phys.*, 78(3):865–951, 2006.

[53] A Greuling, M Rohlfing, R Temirov, FS Tautz, and FB Anders. *arXiv:1009.2020v1*, 2010.

[54] B Coqblin and JR Schrieffer. *Phys. Rev.*, 185(2):847–853, 1969.

[55] N Roch, S Florens, V Bouchiat, and W Wernsdorfer. *Nature*, 453:633, 2008.

[56] N Lorente and JP Gauyacq. *Phys. Rev. Lett.*, 103(17):176601, 2009.

[57] JP Gauyacq, FD Novaes, and N Lorente. *Phys. Rev. B*, 81(16):165423, 2010.

[58] FD Novaes, N Lorente, and JP Gauyacq. *Phys. Rev. B*, 82(15):155401, 2010.

[59] A Mugarza, C Krull, R Robles, R Korytár, N Lorente, and P Gambardella. *submitted*, 2011.

[60] AC Hewson. *The Kondo Problem to Heavy Fermions*. Cambridge studies in magnetism. Cambridge University Press, 1993.

[61] P Nozières and A Blandin. *J. Phys. (Paris)*, 41(3):193–211, 1980.

[62] A Posazhennikova and P Coleman. *Phys. Rev. Lett.*, 94(3):036802, 2005.

[63] A Posazhennikova, B Bayani, and P Coleman. *Phys. Rev. B*, 75(24):245329, 2007.

[64] J Paaske, A Rosch, P Wolfle, N Mason, C M Marcus, and J Nygard. *Nat. Phys.*, 2(2):460 – 464, 2006.

[65] FDM Haldane. *Phys. Rev. Lett.*, 40(6):416–419, 1978.

[66] M Koentopp, K Burke, and F Evers. *Phys. Rev. B*, 73(12):121403, 2006.

[67] AG Borisov, D Teillet-Billy, and JP Gauyacq. *Phys. Rev. Lett.*, 68(18):2842–2845, 1992.

[68] JD Sau, JB Neaton, HJ Choi, SG Louie, and ML Cohen. *Phys. Rev. Lett.*, 101(2):026804, 2008.

[69] DR Hamann and D Vanderbilt. *Phys. Rev. B*, 79(4):045109, 2009.

[70] EM Lifshitz and LD Landau. *Quantum Mechanics: non-relativistic theory*. Pergamon Press, 1977.